Measurement 164 (2020) 108090

Contents lists available at ScienceDirect

Measurement

journal homepage: www.elsevier.com/locate/measurement

Uniaxial ACFM detection system for metal crack size estimation using magnetic signature waveform analysis

Shuxiang Zhao [a], Lingsi Sun [a], Junqi Gao [a,b,c,*], Jiazeng Wang [a], Ying Shen [a,b,c,*]

[a] Acoustic Science and Technology Laboratory, Harbin Engineering University, Harbin 150001, China
[b] Key Laboratory of Marine Information Acquisition and Security (Harbin Engineering University), Ministry of Industry and Information Technology, Harbin 150001, China
[c] College of Underwater Acoustic Engineering, Harbin Engineering University, Harbin 150001, China

ARTICLE INFO

Article history:
Received 8 November 2019
Received in revised form 29 May 2020
Accepted 5 June 2020
Available online 12 June 2020

Keywords:
Single-axis
ACFM detection system
Crack size estimation
Magnetic signature waveform

ABSTRACT

A single-axis alternating current field measurement (ACFM) detection system is proposed for crack size estimation. A single tunneling magneto-resistive (TMR) sensor is used to detect B_z signal, which is able to determine both the length and depth of a crack simultaneously. First, a theoretical analysis is presented to evaluate the crack length and especially depth using B_z signature waveform. The underlying physics principle is supported using a finite element analysis (FEA) method. In the simulation, the cracks with various lengths and depths are analyzed for a given crack width, and corresponding B_z^{max} values are obtained. Next, a B_z^{max} characteristic polynomial surface is developed, which can be represented by a fitted polynomial interpolation equation. The crack depth can be inversed by this equation with reference to the measured B_z^{max} value and crack length. Finally, real ACFM experiments are conducted to demonstrate that the crack lengths and depths can be readily estimated.

1. Introduction

Alternating current field measurement (ACFM), which has evolved from alternating current potential drop (ACPD) and eddy current testing (ECT), represents a non-destructive electromagnetic inspection technology capable of both surface and subsurface (up to skin depth) flaw detection and sizing of conductive metals [1]. Similar to the ECT technique, the ACFM method relies on current-carrying wires to introduce a thin-skin eddy current in the workpiece. However, these two methods use different sensing procedures for inspection of the magnetic field emanating from the load current. Namely, the ECT utilizes a change in the impedance of the current inducer to obtain information on metal surface conditions, while ACFM employs a bi-axial magnetic sensor to gauge magnetic field perturbations caused by a crack. Unlike other detection methods, ACFM can be used in a non-contact manner with no threat to operators. Also, ACFM method does not require coating removal because it is relatively immune to the lift-off effect, clearly demonstrating its merit as a very effective non-destructive testing (NDT) approach [2]. As the most essential role of the NDT technology is quantitative characterization of a failure in critical parts of industrial devices, ACFM has been proven to be effective in a wide range of industries, such as petrochemicals [3], aviation [4], nuclear power plants [5] and railway transportation [6].

In NDT tests, the estimation of the dimensions of a crack profile is of critical concern. Different mathematical models and detection methods have been proposed so far. Shen analyzed the propagation angle of non-vertical surface-breaking cracks and its effect on crack size using a bi-axial Amigo 255 pencil ACFM sensor [7]. Rowshandel presented an artificial neural network-based method for characterization of clustered cracks using two single-axis commercial ACFM sensors [8]. Wu modeled and developed an orthogonal test method for steel wire rope inspection using a tunneling magneto-resistive (TMR) sensor array [9]. Abhishek used an artificial intelligence-based image technique to detect cracks and damages in wind turbine blades using optical fiber sensors [10]. Nicholson proposed a semi-elliptical crack depth sizing inversion method [11]. It indicates that the crack depth could be determined based on the elliptical ratio that fits the $\Delta B_{xmax}/B_{x0}$ value on the condition that a normalized experimental B_x signal and a surface length are known. Espina-Hernandez proposed an eddy current method for crack dimension estimation using a giant magneto-resistive (GMR) sensor [12]. The sensor output's peak-peak value and peak width were employed to quantify the crack widths and depths, respectively. However, the crack length was not taken into account, which is crucial to evaluate and constrain a growing crack, especially during the early stages. Yuan put forward an interpola-

* Corresponding authors at: Acoustic Science and Technology Laboratory, Harbin Engineering University, Harbin 150001, China.
E-mail addresses: gaojunqi@hrbeu.edu.cn (J. Gao), shenying@hrbeu.edu.cn (Y. Shen).

https://doi.org/10.1016/j.measurement.2020.108090
0263-2241/

tion algorithm to estimate both the crack length and depth using the obtained B_x and B_z signal [13,14]. In [15], the pipe crack sizing was realized via a two-step interpolation algorithm using an ACFM testing system. The crack length was measured and calibrated using the B_z signal by a quadratic polynomial interpolation equation in the first step; while the depth of crack was determined according to the B_x signal using a cubic polynomial interpolation equation in the second step. The defect length and depth estimations were realized by two single-axis magnetic sensors manually arranged in an orthogonal manner.

All the mentioned ACFM methods achieved good performance by employing a pair of uniaxial magnetic sensors or multi-axis sensors (or array) to obtain the horizontal and vertical components of the electromagnetic field (B_x and B_z) information. Also, in all these ACFM methods, the crack length was determined based on the B_z curve, while the crack depth is quantized using the B_x curve. However, it is known that there are orthogonal interferences in multi-axis magnetic sensors. The reasons for these interferences are two-fold: (1) it is difficult to deposit a multi-axis sensing element thin-film perfectly in an orthogonal manner during the micro-electromechanical systems (MEMS) manufacturing process; and (2) any two single-axis sensors are unlikely to be right-angle arranged accurately to incorporate a double-axis sensor [16]. For example, it has been reported that the cross-axis effect of a bi-axial MEMS magnetic sensor product is 0.3% with ±3 Gauss magnetic fields on both the sensitive axis and cross-axis [17]. Therefore, using multi-axis sensor leads to inherent system errors, high cost and system complexity. Hence, the limits of available sensor devices inevitably deteriorate the ACFM detection accuracy, which, in combination with mechanical and measurement errors, can escalate the inaccuracy seriously.

To the best of the authors' knowledge, there has been no report on how an unknown crack can be measured using a uniaxial ACFM signal yet. Recently, we reported the analysis of dipole-induced magnetic signature waveform characteristics for target detection and identification [18,19]. In detail, the signature waveform width T was found to be proportional to the closest path approach (CPA) but inversely proportional to the dipole moving speed, which implies that the sensing range angle is independent of changing velocity and CPA. With a change in the motion direction, there is a reversal in its signature waveforms shape. The rich information on peak strength, waveform width and pattern can be used to recognize the target behavior, such as distance, moving velocity and moving direction. Accordingly, we propose a crack dimension evaluation method that uses a single-axis ACFM detection system based on the signature waveform interpretation method. The theoretical study indicates that B_z signature peak value, denoted as B_z^{max}, depends on the crack depth. A typical alternating current with uniform magnitude and direction is induced on the surface of a metal with cracks by an excitation coil, where the magnetic field distortions are created by the perturbation of electric currents around the cracks. A characteristic surface of the ACFM signal is developed based on a FEA simulation model. The single-axis B_z signal can be employed to estimate the dimension of defects using the proposed magnetic signature waveform analysis technique.

The realization of such uniaxial ACFM detection system allows the number of sensors to be halved, especially for array design, reducing the energy consumption and cost of a system by 50%. Moreover, this method eliminates device inherent orthogonal errors, providing a more accurate, streamlined and robust solution for NDT applications. Therefore, a pervasive approach with high detection capability, simple realization and low-power consumption is developed in the harsh environment for underwater NDT testing of pipelines and sea cables.

The contributions of this paper are as follows:

(1) A uniaxial ACFM detection system is proposed to quantify metal surface crack sizes, eliminating the cross-axis errors inherent in a traditional bi-axis sensor system.
(2) An inversion method for the crack size is proposed using the B_z signal in terms of the waveform width and peak value (B_z^{max}). B_z^{max} can serve as a unique indicator to obtain a crack depth by a fitted polynomial interpolation equation.

The rest of the paper is organized as follows. The ACFM physics principles and FEA simulation inversion of a metal surface crack are introduced in Section 2. The crack testing system and the experimental results that verify the feasibility and accuracy of the ACFM method are presented in Section 3. Finally, conclusions are drawn in Section 4.

2. Theoretical analysis

2.1. Physics principle

The principle of ACFM is based on a special case of Maxwell equations that establish the basic laws of electromagnetic field. A figure of the applied current (I) on a good conductor in the presence of a crack is presented in Fig. 1(a), where I in the y-axis direction is confined to flow along the conductor surface due to the skin effect [20–22]. As ACFM is applicable only to good conductors, it is assumed that only the y-component of the electric field intensity, denoted as E_y^z, is traveling along the $+z$ direction, which can be expressed as [23]:

$$E_y^z = E_y^0 e^{-z\sqrt{\pi f \mu \sigma}} \cos(\omega t - z\sqrt{\pi f \mu \sigma}) \tag{1}$$

where z denotes the distance between the interested layer and the conductor surface, E_y^0 is the value of E_y^z at $z = 0$, σ denotes the medium electric conductivity and μ denotes the medium magnetic permeability. For a good conductor, the relationship between the current density $\boldsymbol{J}$ and electrical field $\boldsymbol{E}$ is given by $\boldsymbol{J} = \sigma \boldsymbol{E}$. Then, Eq. (1) can be re-written as:

$$J_y^z = J_y^0 e^{-z\sqrt{\pi f \mu \sigma}} \cos(\omega t - z\sqrt{\pi f \mu \sigma}) \tag{2}$$

where J_y^z denotes the y-component of J traveling along the $+z$ direction, and J_y^0 is the value of J_y^z at $z = 0$. According to Eq. (2), J_y^z declines exponentially with the penetration into the conductor, which is depicted in Fig. 1(a) by the attenuated arrows (green lines) along the z-axis. Further, Eq. (2) implies that variables μ, σ and particularly z jointly affect the strength of J_y^z.

The detection principle of the crack length L by the B_z signature wavelet with a width W is presented in Fig. 1(b). As the current is forced to flow oppositely at both ends of the crack, J_y^z generates reversed curves of B_z. As it is well-known, μ and σ vary the most significantly at the crack boundaries that represent the interface of air and conductor, which creates the densest clockwise and anti-clockwise J_y^z curves, as shown in Fig. 1(b), and which further results in the peak and trough points on B_z curves according to Eq. (2). Therefore, the crack length L can be determined using the wavelet width W of the B_z signature waveforms, as shown in Fig. 1(b).

The detection principle of the crack depth D based on the B_z signature peak value (B_z^{max}) is shown in Fig. 1(c). It is known that magnetic perturbation field B_z is produced by the crack-incurred deflecting part of J_y^z traveling along the $+z$ direction in a range of 0 to D owing to Ampere's law. As a result, the maximum value of B_z (B_z^{max}) can be quantified using the integral of the total direction-changing portion of J_y^z, which is expressed as:

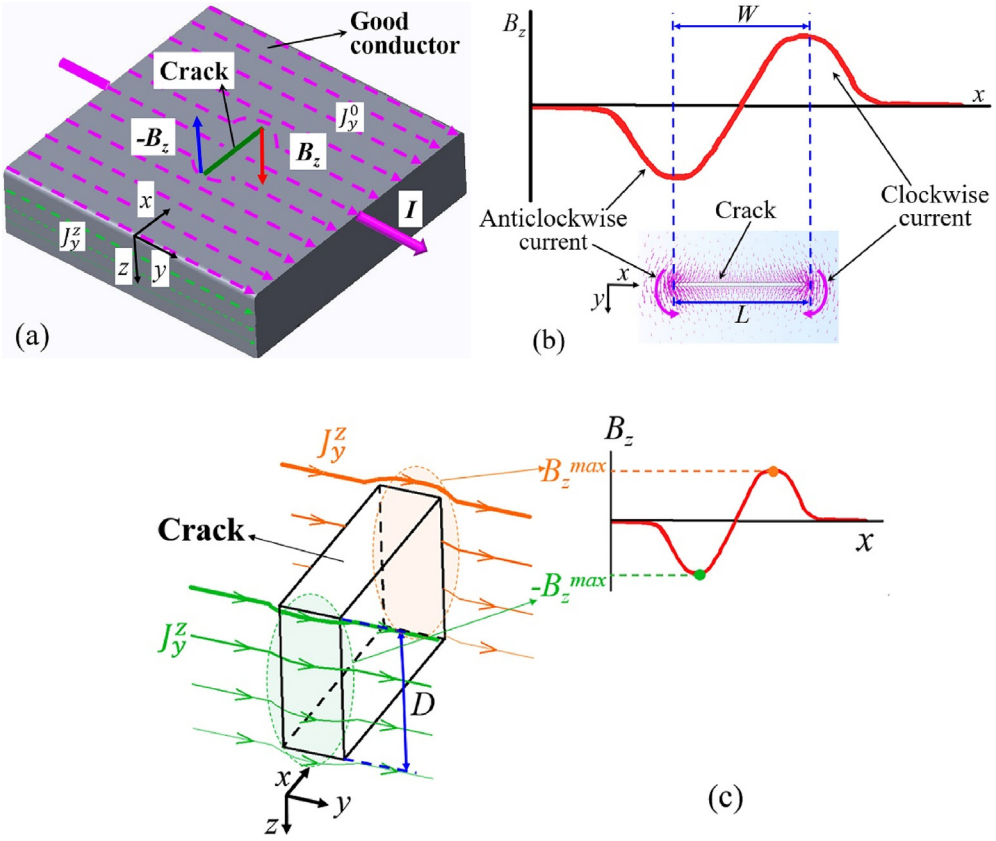

Fig. 1. (a) A picture of the current (I) applied to a good conductor in the presence of a crack. (b) Detection principle of the crack length L by the B_z signature wavelet with a width W. (c) Detection principle of the crack depth D based on the B_z signature peak value B_z^{max}.

$$B_z^{max} = \int_0^D C J_y^z dz \tag{3}$$

where C denotes the rotation coefficient. Eq. (3) indicates that B_z^{max} is dependent on the crack depth D. However, the research interest is to determine the crack depth D based on the B_z^{max} values, which represents an inversion of the relation given by Eq. (3). According to the above analysis, the B_z waveform width and B_z^{max} value can serve as unique indicators to obtain the length and the depth of a crack, respectively. Even though the relationship between the crack length and the ACFM B_z signal is well-known to engineers, the B_z response to a crack depth is still blurred. In order to overcome this problem, the relationship between B_z^{max} and D is studied in detail in Section 2.3.

2.2. Simulation model

In order to better understand the B_z signature waveform caused by a crack, a three-dimensional FEA model was built using the COMSOL 5.3a AC/DC module, as shown in Fig. 2(a). The model consists of a U-shaped excitation probe and an underneath metal specimen with a sequence of cracks; 125 turns of copper wire were wound around an Mn-Zn ferrite yoke with a length of 110 mm and width of 85 mm to introduce a uniform AC field on a mild steel (Q235) specimen. The dimensions of the U-shaped yoke are shown in detail in Fig. 2(b). The crack width was fixed to 0.6 mm, while the length and depth varied. Particularly, the crack length varied from 5 mm to 50 mm with an interval of 5 mm, and the crack depth varied from 1 mm to 11 mm with an interval of 1 mm. The parameters of the FEA model are given in Table 1 and the material properties are shown in Table 2.

A 20 mA alternating sinusoidal current was applied by the excitation coil at frequency of 3 kHz. The orientation of detection was along the crack's centerline from left to right. The detection point was in the middle of the crack's centerline with a lift-off of 1 mm, labeled in red in Fig. 2(a). The magnetic density of the z-component B_z was extracted at the detection point. Parametric scanning means were used to solve and analyze the required magnetic field distribution around the crack. The detection point moved with the yoke so that their relative position was constant.

The induced current was confined in the surface layer of the steel flat due to the skin effect. The skin depth of the specimen was 0.23 mm, and it was calculated and set according to $\delta = \sqrt{1/\pi f \mu \sigma}$, where δ denotes the skin depth.

2.3. Signature waveform analysis

The effect of the crack depth on the B_z signal was first examined at a fixed crack length of L = 30 mm. The group of B_z curves at different depths of D ranging from 1 to 11 mm with a step 1 mm is presented in Fig. 3(a). As expected, the widths of each pair of peak and troughs of all the curves were measured to be 27.5 mm, which were direct reflections of the crack lengths of 30 mm. It should be noted that different crack depths corresponded to different B_z^{max} values that increased as the crack depth D increased from 1 to 11 mm; this is in accordance with the principle analysis presented in Section 2.1. Therefore, the depth information can be extracted from the B_z signature waveforms, which can be exploited comprehensively to estimate the crack dimensions.

Next, the effect of the crack length was analyzed at a fixed depth of D = 6 mm and variable L, where L ranged from 5 to 50 mm at increments of 5 mm. The obtained B_z curves are pre-

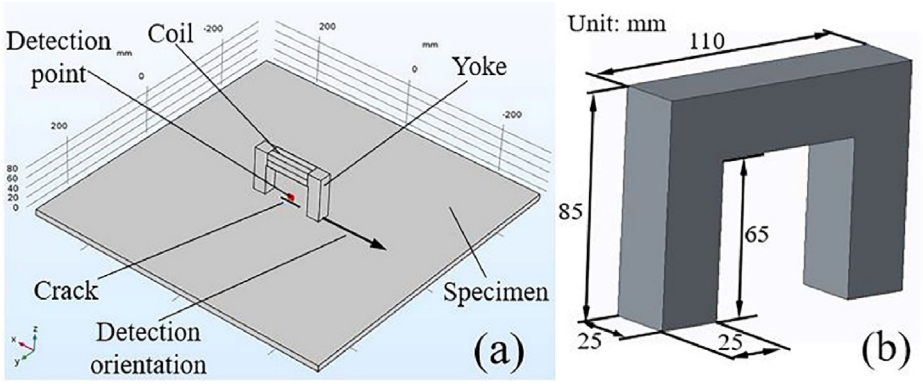

Fig. 2. (a) 3D FEA model of the ACFM. (b) Dimensions of the U-shaped yoke.

Table 1
Parameters of the 3D FEA model.

Model	Diameter (mm)	Length (mm)	Width (mm)	Depth (mm)
Specimen	–	600	600	12
Yoke	–	110	25	85
Crack	–	–	0.6	–
oil	0.41	60	25	25
Air	–	1500	1500	800

Table 2
Material properties of the 3D FEA model.

Model	Material	Relative permeability	Conductivity (S/m)
Specimen	Mild steel (Q235)	240	6.67×10^6
Yoke	Mn-Zn ferrite	3000	0.1
Coil	Copper	1	5.95×10^7

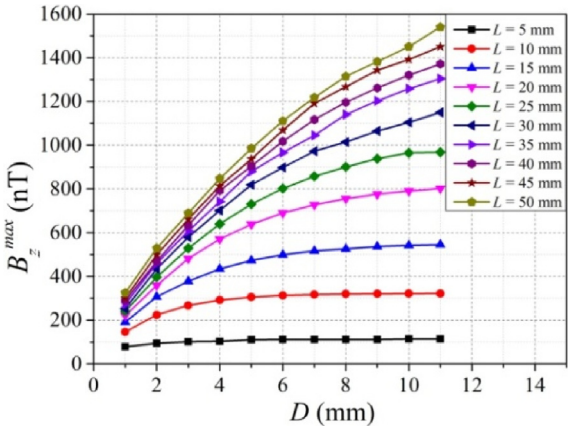

Fig. 4. The B_z^{max} response dependence on the crack depth D at different crack lengths L.

sented in Fig. 3(b), where it can be seen that the information from the peak and trough widths can be used to predict the flaw length. In particular, it was found that the B_z^{max} values became more intensive as L increased. The simulation results showed that the peak widths of B_z waveforms and B_z^{max} values could be used to estimate the flaw length and depth.

A sequence of B_z^{max} responses as a function of the crack depth D at different crack lengths L are presented in Fig. 4, where it can be seen that B_z^{max} values increased first quickly and then slowly with the crack depth D. Furthermore, in Fig. 4, it can be observed that B_z^{max} values increased with the crack length L when $5 \leq L \leq 50$ mm. Also, greater change rates of B_z^{max} curves suggested larger cracks. It should be noted that there was no overlap between the curves, which indicates that B_z^{max} value is a unique indicator of a specific crack with good one-to-one correspondence. Therefore, by extracting information on L using the wavelet width W, it is feasible to employ B_z^{max} values to predict the value of D.

By virtue of the simulated data presented above, a magnetic characteristic polynomial surface was mapped using Matlab software, and the result is illustrated in Fig. 5. It can be clearly seen

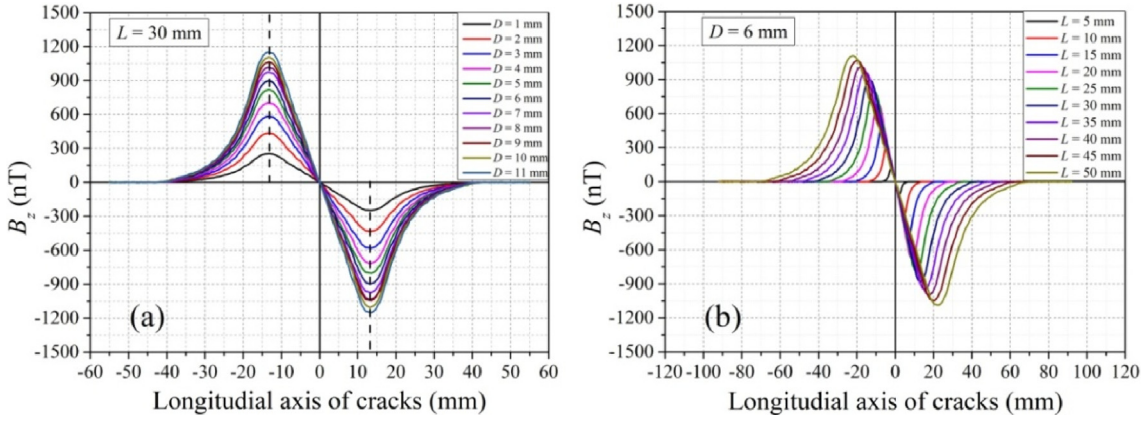

Fig. 3. (a) Simulated magnetic signal B_z at L = 30 mm and D ranging from 1 to 11 mm with a step 1 mm. (b) Simulated magnetic signal B_z at D = 6 mm and L ranging from 5 to 50 mm at 5 mm increments.

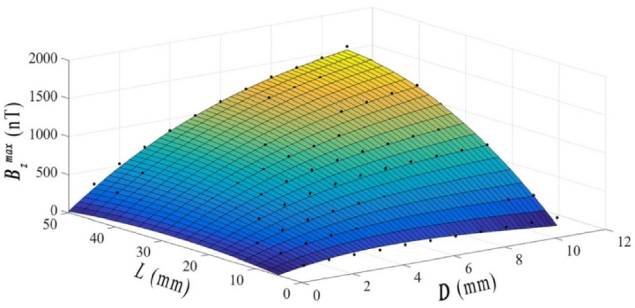

Fig. 5. Magnetic characteristic surface based on simulated data.

that the B_z^{max} value initially increased quickly as the length and depth of a crack increased, and then the fitted surface leveled off as the crack size further increased. It should be noted that there was no jump or distortion on the numerical surface, making it achievable to express the actual crack profiles. The characteristic surface was represented by a fitted polynomial interpolation as follows:

$$B_z{}^{max} = -33.49 + 35.26D + 9.672L - 8.931D^2 + 6.568DL - 0.1716L^2 + 0.3157D^3 - 0.1165D^2L - 0.0423DL^2 \quad (4)$$

where B_z^{max} refers to the peak value of B_z in the unit of nT.

In the Matlab fitting process, a Bisquare approach was used to improve the robustness of the fitting equation. The degree of D was found to be cubic, whereas the degree of L was square on the surface. With reference to the measured B_z^{max} and L values, the crack depth D could be inversed using the polynomial surface equation. This indicates that the characteristic B_z signature waveform can be used to estimate both the length and the depth of a crack. Therefore, a straightforward interpolation algorithm solution is provided so that only the B_z signal is required, eliminating the need for the B_x signal in the crack size estimation. It should be noted that the magnetic characteristic subsurface cracks were not considered. Accordingly, by introducing the subsurface crack inversion in the proposed method, the measurement results of the crack depth estimation could be affected.

3. Experimental verification

3.1. Single-axis ACFM detection system

A photograph of a single-axis ACFM detection system is shown in Fig. 6(a). The probe consisted of a U-shape non-ferromagnetic yoke, a coaxial excitation coil wound around the yoke, and a single-axis TMR sensor, as shown in Fig. 6(b). The detecting sensor was customized using a TMR sensing element, and the corresponding voltage amplifier circuit was designed using a gain transfer function of 100× over a high-pass filter of f > 160 Hz. Being energized by a DC power supplier (E36311A, Keysight, USA) with a 2.5 V voltage bias, the TMR sensor was attached to the probe,

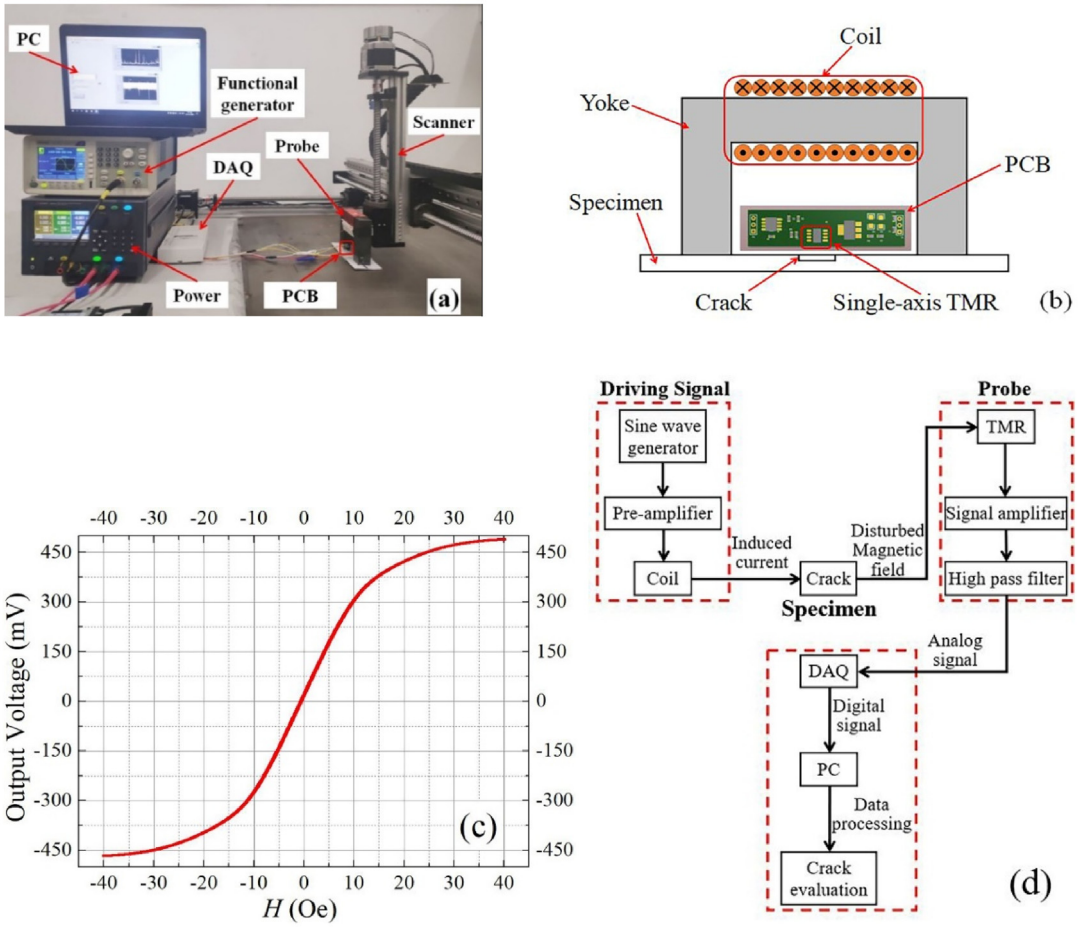

Fig. 6. (a) Photograph of the single-axis ACFM detection system. (b) Side-view of the single-axis TMR sensor probe. (c) Sensitivity curve of the used TMR sensing element. (d) Block diagram of the experimental system.

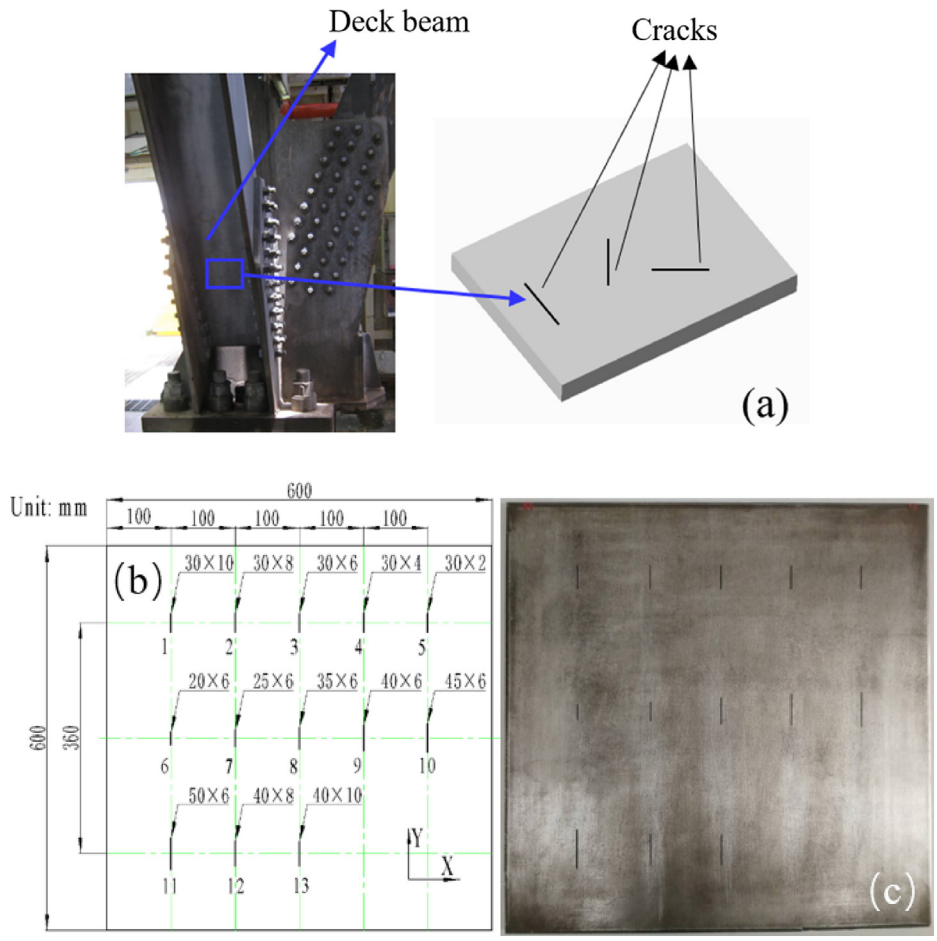

Fig. 7. (a) Schematic picture of the cracks on a deck beam. (b) Workpiece design. (c) Top view of the workpiece.

which was driven by a scanner passing over the metal workpiece with a lift-off of 1 mm. The magnetic field sensitivity of the TMR sensor (MultiDimension Technology, China) was characterized as a function of the magnetic field (H) along the sensing axis using a pair of electromagnets. As shown in Fig. 6(c), the sensitivity of the TMR sensor was 30 mV/V/Oe, which was determined by the slope of the transfer curve in a linear range of H = ±10 Oe. The dimensions and parameters of the coil and yoke were the same as those used in the previous simulation (see Table 1). The impedance of the current-carrying coil was measured by an impedance analyzer (E4990A, Keysight, USA) to be 90.375 Ω at 3 kHz. A peak-peak voltage (V_{PP}) of a 2.5 V excitation signal at frequency of 3 kHz was applied to the coil, provided by a functional generator (AFG1022, Tektronix, USA). The analog sensor output signal was sent to a datalogger (USB6210, National Instrument, USA) for data acquisition. The discrete signal was then processed and analyzed by Labview for crack size evaluation. The block diagram of the experimental system is illustrated in Fig. 6(d).

A group of cracks on a deck beam in the real application is shown schematically in Fig. 7(a). As illustrated in Fig. 7(b), a mild steel plate (Q235B) of 600 mm × 600 mm × 12 mm was used as a target workpiece. The design scheme was realized using electrical discharge machining (EDM), including a group of thirteen strip notches of the same width of 0.6 mm, which served as actual defects. Samples 1, 2, 3, 4 and 5 had a length of L = 30 mm but different depths of D = 10, 8, 6, 4 and 2 mm, respectively. Samples 6 – 11 had a fixed depth of D = 6 mm and different lengths of L = 20, 25, 35, 40, 45 and 50 mm, respectively. Samples 12 and 13 had the same length of L = 40 mm and different depths of D = 8 and 10 mm, respectively. The distances between two adjacent crack central points were 100 mm along the x-axis and 180 mm along the y-axis. A top view picture of the workpiece is shown in Fig. 7 (c). The probe on the top of cracks moved at a constant velocity of 5 mm/s, allowing the sensor to detect the magnetic signal appropriately.

3.2. Experimental results

The effect of the crack depth was first examined by scanning the first-row notches (No. 1, 2, 4 and 5). The width of No. 3 was measured to be 0.5 mm, while its designed value was 0.6 mm. This difference was caused by an imperfection of the notch machining process, and therefore, it was excluded from the analysis of the experimental results. The probe was moved along the longitudinal direction (y-axis) of each crack, and the results are shown in Fig. 8 (a). As expected, the measured crack lengths (L') obtained by the distances between the waveform peaks and troughs were 29.0, 28.5, 28.5 and 29.5 mm, which were all close to the crack length value of 30 mm. Based on the obtained B_z fingerprint waveforms, the B_z^{max} values were determined to be 80.5, 77.0, 50.2 and 34.1 mV. It was found that deep crack depths led to the large B_z^{max} values, and the changing trends of these curves coincided well with the simulated results, as illustrated in Fig. 3(a). In order to verify the feasibility of the proposed single-axis interpolation algorithm, Eq. (4) was converted into the unit of mV using the sensor's sensitivity of 30 mV/V/Oe and the supply voltage of 2.5 V, which yielded to the following relationship:

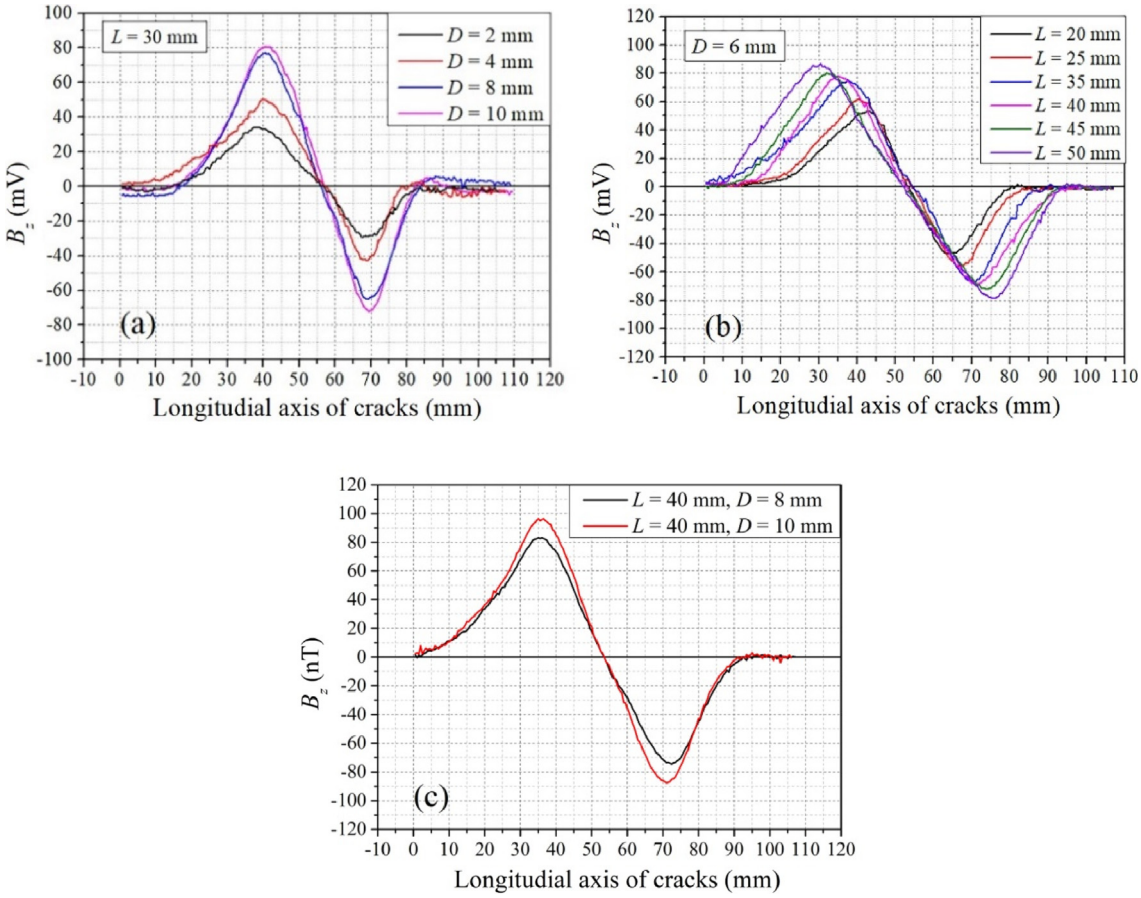

Fig. 8. Experimental results. (a) Experimental magnetic signal B_z at constant L of 30 mm and variable D of 10, 8, 4 and 2 mm, respectively. (b) Experimental magnetic signal B_z at constant D of 6 mm and variable L of 20, 25, 35, 40, 45 and 50 mm, respectively. (c) Experimental magnetic signal B_z of cracks 12 and 13.

Table 3
Test results of crack dimensions.

No.	L (mm)	L' (mm)	D (mm)	B_z^{max} (mV)	D' (mm)	D_{error} (%)
1	30	29.0	10	80.5	9.3	7.00
2	30	28.5	8	77.0	8.6	7.50
4	30	28.5	4	50.2	3.9	2.50
5	30	29.5	2	34.1	2.1	5.00
6	20	21.5	6	53.4	6.3	5.00
7	25	26.5	6	61.9	6.0	0.00
8	35	33.0	6	75.3	6.6	10.00
9	40	36.5	6	77.9	6.3	5.00
10	45	40.5	6	80.3	6.1	1.67
11	50	45.5	6	86.4	6.4	6.67
12	40	36.5	8	82.9	7.1	11.25
13	40	36.0	10	96.4	10.0	0.00

$$B_z{}^{max} = -2.512 + 2.645D + 0.725L - 0.67D^2 + 0.493DL - 0.013L^2 + 0.024D^3 - 0.009D^2L - 0.003DL^2 \quad (5)$$

It should be noted that Eq. (5) was used only to predict the dimensions of surface crack. However, if there is a subsurface crack, Eq. (5) is not applicable and certain corrections should be made considering the defect sub-superficiality degree, i.e., the distance from the material surface to that of the defect.

By substituting the measured data of B_z^{max} and L' into Eq. (5), the estimated crack depth D' of cracks 1, 2, 4 and 5 was calculated to be 9.3, 8.6, 3.9 and 2.1 mm, which corresponded to the crack depth error (D_{error}) of 7.00%, 7.50%, 2.50% and 5.00%, respectively. These results showed that the accuracy of the crack-size estimation was independent of the crack depth. The real and estimated values of the crack dimensions are provided in Table 3.

The role of crack length was further analyzed using No. 6–11 notches, and the corresponding B_z curves are presented in Fig. 8 (b), where the B_z curves became wider as L increased. In particular, the distances between each peak and trough pair were measured to be 21.5, 26.5, 33.0, 36.5, 40.5 and 45.5 mm, which were direct reflections of the crack lengths of 20, 25, 35, 40, 45 and 50 mm, respectively; the corresponding B_z^{max} values were 53.4, 61.9, 75.3, 77.9, 80.3 and 86.4 mV, as given in Table 3. By substituting the values of B_z^{max} and L' into Eq. (5), the estimated depth D' values were obtained, and they were 6.3, 6.0, 6.6, 6.3, 6.1 and 6.4 mm, which corresponded to D_{error} of 5.00%, 0.00%, 10.00%, 5.00%, 1.67% and

6.67%, respectively. Accordingly, the prediction accuracy of the crack damage level was good and independent of changes in the value of L.

Unlike the other cracks, the dimensions of the last two cracks (No. 12 and No. 13) were not considered in advance in the simulation model. Their B_z signature waveforms are shown in Fig. 8(c). The values of L' and B_z^{max} were determined to be 36.5 mm and 82.9 mV for crack No. 12, and 36.0 mm and 96.4 mV for crack No. 13, respectively. The substitution of values of L' and B_z^{max} into Eq. (5) resulted in D' values of 7.1 mm and 10.0 mm for cracks No. 12 and No. 13, respectively, which corresponded to D_{error} of 11.25% and 0, as shown in Table 3.

Therefore, the measured wavelet peak-trough width (L) and peak value (B_z^{max}) could be used to determine the value of D using the interpolation equation. Although the experimental results did not demonstrate an extremely precise determination of D values, the depth errors were in the acceptable range and supportive of the proposed evaluation method. The simulation and experimental results demonstrate that the uniaxial B_z signature waveform represents a promising determination technology of length and depth of a crack.

It should be noticed that, in this work, Eq. (5) was used adopting certain premises, i.e., the crack width was fixed at 0.6 mm. However, in the case of a varying fatigue width, Eq. (5) is not applicable, so the corresponding characteristic surface should be developed, and experimental measurements and a new interpolation equation will show significant differences.

4. Conclusion

Despite the consensus about the advantage of ACFM schemes, there is significant room for system improvement in real applications. More robust and simple probe devices and accurate fatigue characterization techniques are of utmost interest in the community. In view of that, in this paper we present an evaluation method to interpret the crack profile based on a single-axis sensor method. The obtained B_z signature waveform can be interpreted comprehensively to estimate both the crack length L and the crack depth D. Theoretical analysis indicates that B_z^{max} is quantified by the integral of the total deflecting current density of the y-component traveling along the $+z$ direction J_y^z, making B_z^{max} dependent on the crack depth D. A FEA model was developed to study the magnetic characteristic signal with a fixed crack width. A B_z^{max} interpolation surface obtained from the numerical simulation was mapped with respect to the length and depth of a crack (L and D). As L can be directly predicted based on the B_z signal waveforms width, D can be readily interpreted by the peak strength B_z^{max} interpolation algorithm via inversion. The validity of the proposed methodology was verified experimentally, and an accurate estimation of the value of D was achieved.

Unlike the original ACFM method, the proposed method uses the B_z signal as a unique cue, which provides a more straightforward and faster crack size detection. Moreover, the proposed ACFM method provides an accurate, low-cost, compact-size, and low-power test solution, which is the first step towards the optimization of a detection system. At present, we are designing a single-axis ACFM sensor array probe for underwater equipment surface and subsurface crack sizing, which will be presented in our future work.

CRediT authorship contribution statement

Shuxiang Zhao: Conceptualization, Methodology, Investigation, Writing - original draft. **Lingsi Sun:** Data curation, Software. **Junqi Gao:** Funding acquisition, Supervision. **Jiazeng Wang:** Software, Validation. **Ying Shen:** Funding acquisition, Supervision, Writing - review & editing.

Declaration of Competing Interest

The authors declare that they have no known competing financial interests or personal relationships that could have appeared to influence the work reported in this paper.

Acknowledgments

This work was supported in part by the Natural Science Foundation of Heilongjiang Province of China (LH2019E040) and the Academy of Space Electronic Information Technology (6142411183410). The work was also supported by Acoustic Science and Technology Laboratory Grant (JCKYS2019604SSJS005, JCKYS2020604SSJS006).

References

[1] B. Blakeley, M. Lugg, ACFM: application of ACFM for inspection through metal coatings, Insight: Non-Destruct. Test. Cond. Monit. 52 (2010) 310–315.
[2] R.K. Amineh, M. Ravan, S.H.H. Sadeghi, R. Moini, Using AC field measurement data at an arbitrary liftoff distance to size long surface-breaking cracks in ferrous metals, NDT E Int. 41 (2008) 169–177.
[3] B. Blakeley, M. Lugg, Recent research and development activities in electromagnetic sensor technologies, Insight: Non-Destruct. Test. Cond. Monit. 53 (2011) 138–141.
[4] M.C. Lugg, Applications of A.C. field measurement techniques for the aircraft industry, Aircraft Eng. Aerosp. Technol. 62 (1990) 9–11.
[5] M. Smith, C. Laenen, Inspection of nuclear storage tanks using remotely deployed ACFMT, Insight: Non-Destruct. Test. Cond. Monit. 49 (2007) 17–20.
[6] J.M. Chacón Muñoz, F.P. García Márquez, M. Papaelias, Railroad inspection based on ACFM employing a non-uniform B-spline approach, Mech. Syst. Sig. Process. 40 (2013) 605–617.
[7] J.L. Shen, L. Zhou, H. Rowshandel, G.L. Nicholson, C.L. Davis, Determining the propagation angle for non-vertical surface-breaking cracks and its effect on crack sizing using an ACFM sensor, Meas. Sci. Technol. 26 (2015) 115604.
[8] H. Rowshandel, G.L. Nicholson, J.L. Shen, C.L. Davis, Characterisation of clustered cracks using an ACFM sensor and application of an artificial neural network, NDT E Int. 98 (2018) 80–88.
[9] B. Wu, Y.J. Wang, X.C. Liu, C.F. He, A novel TMR-based MFL sensor for steel wire rope inspection using the orthogonal test method, Smart Mater. Struct. 24 (2015) 075007.
[10] A. Reddy, V. Indragandhi, L. Ravi, V. Subramaniyaswamy, Detection of Cracks and damage in wind turbine blades using artificial intelligence-based image analytics, Measurement 147 (2019) 106823.
[11] G.L. Nicholson, C.L. Davis, Modelling of the response of an ACFM sensor to rail and rail wheel RCF cracks, NDT E Int. 46 (2012) 107–114.
[12] J.H. Espina-Hernández, E. Ramírez-Pacheco, F. Caleyo, J.A. Pérez-Benitez, J.M. Hallen, Rapid estimation of artificial near-side crack dimensions in aluminium using a GMR-based eddy current sensor, NDT and E Int. 51 (2012) 94–100.
[13] W. Li, X. Yuan, G. Chen, X. Yin, J. Ge, Induced circumferential current for transverse crack detection on a pipe string, Insight: ACFM 57 (2015) 528–533.
[14] X. Yuan, W. Li, G. Chen, X. Yin, J. Ge, W. Jiang, J. Zhao, Bobbin coil probe with sensor arrays for imaging and evaluation of longitudinal cracks inside aluminum tubes, IEEE Sens. J. 18 (2018) 6774–6781.
[15] X. Yuan, W. Li, G. Chen, X. Yin, W. Yang, J. Ge, Two-step interpolation algorithm for measurement of longitudinal cracks on pipe strings using circumferential current field testing system, IEEE Trans. Ind. Inf. 14 (2018) 394–402.
[16] V.S. Luong, J.-T. Jeng, C.-C. Lu, H.-Y. Hsu, Low-noise tunneling-magnetoresistance vector magnetometers with flux chopping technique, Measurement 109 (2017) 297–303.
[17] H. Corporation, 1- and 2-Axis Magnetic Sensors HMC1001/1002/1021/1022, 2020, pp. 4.
[18] Y. Shen, J. Wang, J. Shi, S. Zhao, J. Gao, Interpretation of signature waveform characteristics for magnetic anomaly detection using tunneling magnetoresistive sensor, J. Magn. Magn. Mater. 484 (2019) 164–171.
[19] Y. Shen, D. Hasanyan, J. Gao, Y. Wang, J. Li, D. Viehland, A magnetic signature study using magnetoelectric laminate sensors, Smart Mater. Struct. 22 (2013) 095007.
[20] H. Saguy, D. Rittel, Bridging thin and thick skin solutions for alternating currents in cracked conductors, Appl. Phys. Lett. 87 (2005) 084103.
[21] A.M. Lewis, R. Collins, D.H. Michael, The thin-skin electromagnetic field near a surface crack in a ferromagnetic metal, Rev. Prog. Quant. Nondestruct. Eval. 9A (1990) 273–280.
[22] A. Akbari-Khezri, S.H.H. Sadeghi, R. Moini, M. Sharifi, An efficient modeling technique for analysis of AC field measurement probe output signals to improve crack detection and sizing in cylindrical metallic structures, J. Nondestr. Eval. 35 (2015) 9.
[23] W.H. Hayt, J.A. Buck, Engineering Electromagnetics, eighth ed., McGraw-Hill Companies Inc, New York, 2012.